A study of the ionogram derived effective scale height around the ionospheric hmF2

L. Liu, W. Wan, B. Ning

Ann. Geophys., 24, 851–860, 2006
www.ann-geophys.net/24/851/2006/

Annales Geophysicae

A study of the ionogram derived effective scale height around the ionospheric *hm*F2

L. Liu, W. Wan, and B. Ning

Institute of Geology and Geophysics, Chinese Academy of Sciences, Beijing 100029, China

Received: 19 August 2005 – Revised: 9 February 2004 – Accepted: 23 February 2006 – Published: 19 May 2006

Abstract. The diurnal, seasonal, and solar activity variations of the ionogram derived scale height around the ionospheric F-layer peak (Hm) are statistically analyzed at Wuhan (114.4° E, 30.6° N) and the yearly variations of Hm are also investigated for Wuhan and 12 other stations where Hm data are available. Hm, as a measure of the slope of the topside electron number density profiles, is calculated from the bottomside electron density profiles derived from vertical sounding ionograms using the UMLCAR SAO-Explorer. Results indicate that the value of median Hm increases with increasing solar flux. Hm is highest in summer and lowest in winter during the daytime, while it exhibits a much smaller seasonal variation at night. A common feature presented at these 13 stations is that Hm undergoes a yearly annual variation with a maximum in summer during the daytime. The annual variation becomes much weaker or disappears from late night to pre-sunrise. In addition, a moderate positive correlation is found between Hm with *hm*F2 and a strong correlation between the bottomside thickness parameter B0 and Hm. The latter provides a new and convenient way for empirical modeling the topside ionospheric shape only from the established B0 parameter set.

Keywords. Ionosphere (Modeling and forecasting; Solar radiation and cosmic ray effects; General or miscellaneous)

1 Introduction

Knowledge of the spatial distribution of the electron density in the ionosphere, especially the ionospheric profile $N_e(h)$, is important for scientific interest, such as ionospheric empirical modelings and ionospheric studies, and for practical applications for time delay correction of the radio wave propagation through the ionosphere, etc. During the past decades, great efforts have been made in the global ionospheric empirical modeling (Bilitza, 2001). Many mathematical functions, such as the Chapman, exponential, parabolic, Epstein functions, have been proposed to describe the ionospheric profiles (e.g. Booker, 1977; Rawer et al., 1985; Rawer, 1988; Di Giovanni and Radicella, 1990; Stankov et al., 2003). Among these functions, the Chapman function is simple and has great potential for analytical modeling of the ionospheric profile (e.g. Huang and Reinisch, 2001). A nice feature of the Chapman profiler is that it only needs information about the electron density and height of the F peak and scale height to give a good representation for the observed topside $N_e(h)$. Studies have identified that the Chapman function, even with a constant scale height, fits the topside ionospheric profile well several hundred kilometers above the F2-peak (Reinisch and Huang, 2004; Belehaki et al., 2003). This is enough for most situations because most electrons in the ionosphere are distributed in this region. When the scale height is linearly varied with height, the fit will be greatly improved in the higher region (Lei et al., 2005).

It is evident that the scale height is a key and inherent parameter for ionospheric profiles, especially for the topside profiler (Stankov et al., 2003; Belehaki et al., 2006). However, there are still limited studies on the behavior of the plasma scale height. Recently, Huang and Reinisch (2001) introduced a new technique to extrapolate the topside ionosphere based on information from ground-based ionogram measurements. They approximated the $N_e(h)$ both around and above the F2-layer peak (*hm*F2) by an α-Chapman function with a scale height (Hm) determined at *hm*F2. The parameter Hm derived from ionograms is a measure of the electron density profile slope of the topside ionosphere. The Hm data is routinely archived at some stations after being derived from the Digisonde ionograms with the UMLCAR SAO-Explorer (http://ulcar.uml.edu/).

In this paper, we conduct a statistical analysis on the variations of the ionogram derived scale height (Hm) around the F2-peak during 1999–2004 from routine

Correspondence to: L. Liu
(liul@mail.iggcas.ac.cn)

Published by Copernicus GmbH on behalf of the European Geosciences Union.

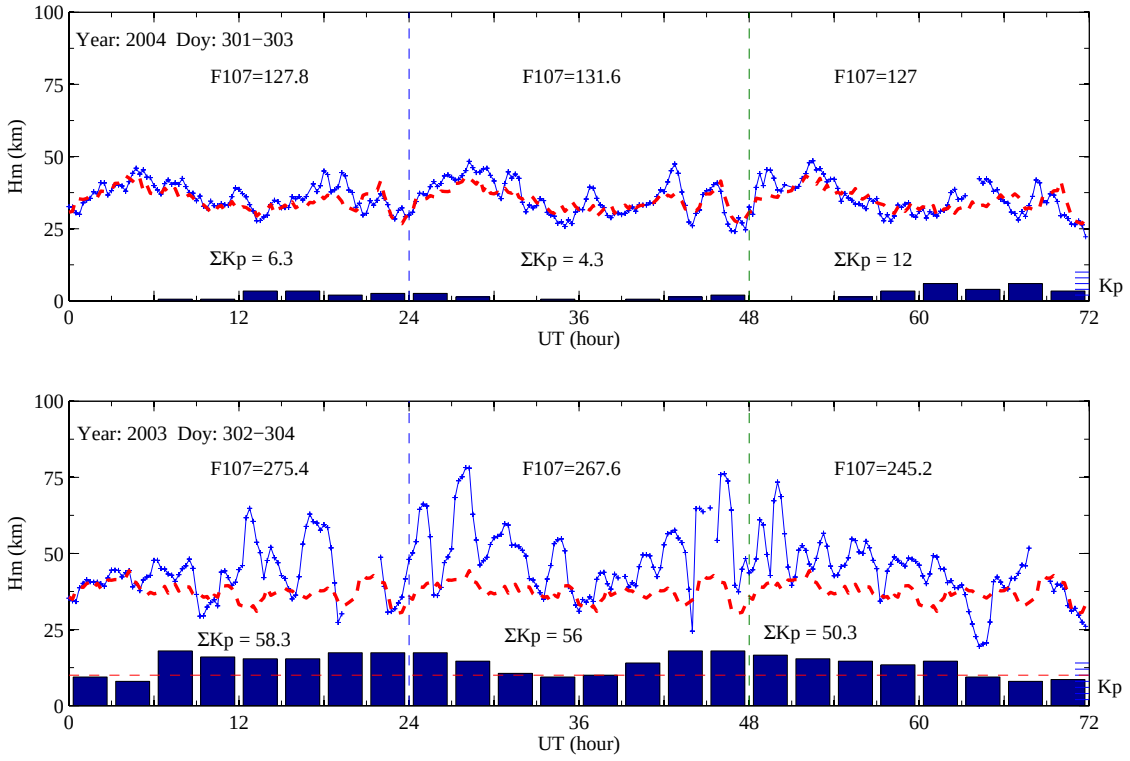

Fig. 1. Diurnal variations of the scale height (Hm) derived from Digisonde measurements recorded at Wuhan during 29–31 October 2003 and 27–29 October 2004. The median values of Hm in the nearest 31 days are plotted in dashed lines for a reference. The 3-hour K_p index is illustrated in the histograms. The corresponding daily sum K_p and solar index F107 indices are also labeled. Local Time, LT, is UT plus 7.6 h at Wuhan.

Digisonde measurements recorded at Wuhan (geographic 114.4° E, 30.6° N; 45.2° dip), China, and on the yearly variations of Hm observed at Wuhan, College (64.9° N, 212.2° E), Narssarssuaq (61.2° N, 314.6° E), Chilton (51.6° N, 358.7° E), Millstone Hill (42.6° N, 288.5° E), Tortosa (40.4° N, 0.3° E), Athens (38° N, 23.5° E), Wallops Is. (37.8° N, 284.5° E), Ascension Is. (7.9° S, 345.6° E), Madimbo (22.4° S, 30.9° E), Louisvale (28.5° S, 21.2° E), Grahamstown (33.3° S, 26.5° E) and Port Stanley (51.7° S, 302.2° E) stations. The results will have empirical modeling applications.

2 Data

The present analysis uses a database of Hm observed at Wuhan, College, Narssarssuaq, Chilton, Millstone Hill, Tortosa, Athens, Wallops Is., Ascension Is., Madimbo, Louisvale, Grahamstown and Port Stanley. To investigate the annual variation, Hm data at the latter 12 stations were downloaded from the SPIDR web (http://spidr.ngdc.noaa.gov/spidr/).

More than 219 000 ionograms were routinely recorded at Wuhan (China) with a DGS-256 Digisonde during 1999–2004. A huge effort has been made to manually scale those ionograms, and the bottomside profiles are calculated from these hand-scaling ionograms with a standard "true height" inversion program (Reinisch and Huang, 1983; Huang and Reinisch, 1996) inherent in the UMLCAR SAO-Explorer. The critical frequency (*fo*F2) and its height (*hm*F2) of the F-layer, the IRI bottomside profile thickness parameter B0, etc., are obtained. At the same time, the scale height around the F2-peak (Hm) is also derived. The calculation of Hm from the bottomside profile can be found in the work of Huang and Reinisch (2001) and Reinisch and Huang (2004). B0 is a bottomside thickness parameter that gives the height difference between *hm*F2 and the height where the electron density profile has dropped down to 0.24**Nm*F2.

3 Results and discussions

3.1 Daily variation and geomagnetic dependence of Wuhan Hm

There are appreciable diurnal and day-to-day variations in the ionogram derived scale height around the F2-peak, Hm, derived from Digisonde measurements. Figure 1 displays Hm recorded at Wuhan for three geomagnetically disturbed days (29–31 October 2003) and three quiet days

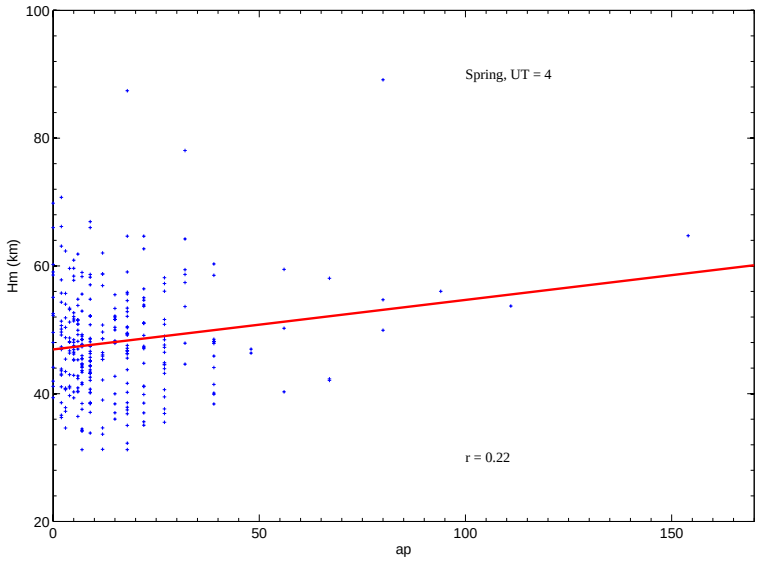

Fig. 2. Scatterplot of the scale height (Hm) at Wuhan versus the 3-h geomagnetic activity index ap at 04:00 UT (around local noon) in spring. The solid line shows the trend of the linear regression.

(27–29 October 2004). The median values of Hm in the nearest 31 days are also plotted with dashed lines which serve as a reference level.

Hm for those three quiet days (27–29 October 2004) in general follows the average behavior. In contrast, for three geomagnetically disturbed days (29–31 October 2003), the variability of Hm is enhanced and it significantly deviated from the median behavior. This indicates the redistribution of the ionospheric ionization during geomagnetic disturbances due to the storm impact. Thus, for constructing a complete ionospheric image during storms, Hm may present complementary characteristics of the ionosphere.

The effects of geomagnetic storms on the ionosphere are well-known to be complicated and stochastic. The geomagnetic dependence of Hm at Wuhan has been statistically investigated with the planetary geomagnetic indices, 3-hour K_p and A_p, and the daily K_p and A_p. Although Hm may greatly deviate from the average pattern under individual disturbed situations, the correlations of Hm with these indices are poor, as depicted in Fig. 2. It implies a complicated dependence of Hm on geomagnetic activity. Furthermore, it also suggests insignificant differences in the averaged values of Hm at specified times for those 6 years if we separate the data into two groups, low ($A_p<15$) and moderate to high ($A_p>15$) magnetic activity levels.

3.2 Seasonal and solar activity variations of Wuhan Hm

Several atmospheric and ionospheric parameters display regular seasonal and solar activity variations (e.g. Richards, 2001; Lei et al., 2005). At low and middle latitudes, the primary source of ionization in the F-region is the EUV solar irradiances. The solar activity dependence of ionospheric characteristics has been studied in the early various ionospheric observations. Richards et al. (1994) have shown that the solar cycle variation of most solar EUV flux lines can be scaled accurately enough for aeronomic applications by using F107p = (F107 + F107A)/2, where F107A is the 81-day running mean of daily F107 index. Now we use F107p as an indicator of the solar activity level in this analysis.

Figure 3 presents the mothly diurnal variation of Hm at Wuhan in 2002. The average and day-to-day variability of the monthly Hm is described by the corresponding median and upper and lower quartiles, which are represented in lines with vertical bars, respectively. It can be observed from the figure that the values of median Hm vary from 30–80 km. As seen from Fig. 3, Hm are roughly of a similar behavior in the months from November to February. It is true for Hm grouped in March and April, May to August, and September and October, respectively. Thus, to look for their seasonal variation, the parameters in months from November to February are classified as winter, March and April as spring, May to August as summer, and September and October as autumn, respectively.

Diurnal variations of the median Hm for four seasons under high (F107p>180) and moderate-to-low (F107p<140) solar activity levels are plotted in Fig. 4. In Fig. 4, data are grouped according to their solar activity levels. The possible influence of geomagnetic activities is not excluded.

Under moderate-to-low and high solar activities, a morning increase in Hm is followed by an afternoon decrease. There is no significant change in Hm during the nighttime compared with the daytime, except for a small peak in the winter under high solar activity. In summer, Hm has a

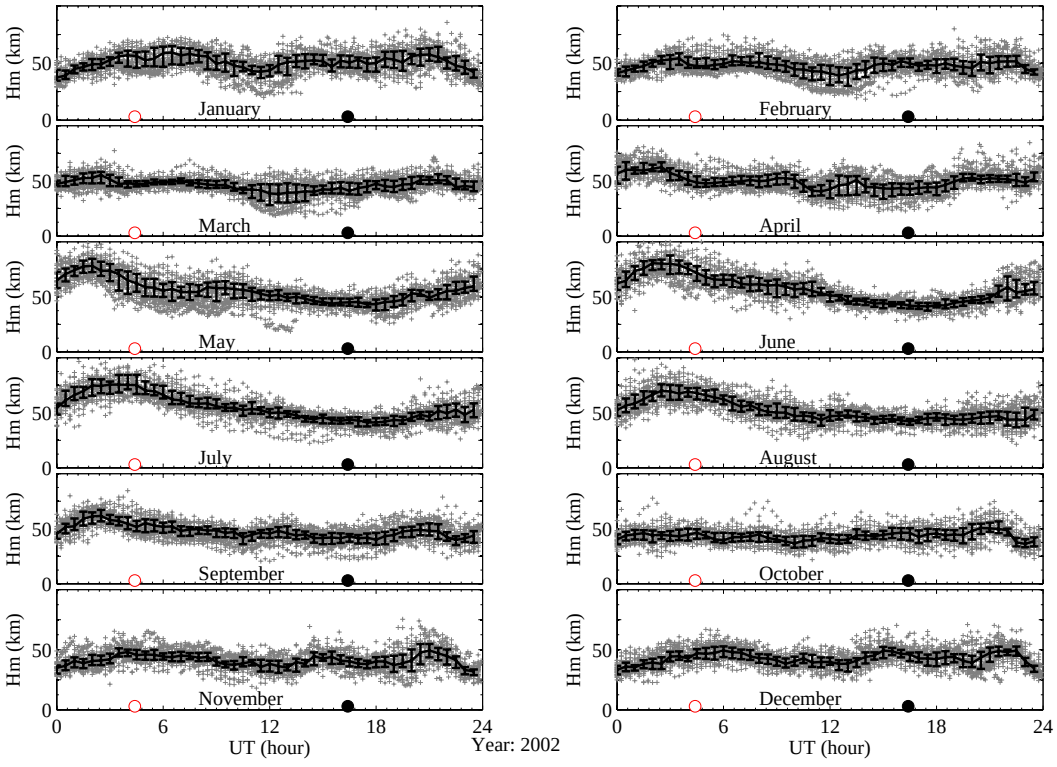

Fig. 3. Diurnal variations of Hm at Wuhan in 2002. Lines with bars, respectively, represent the monthly median values of Hm and the corresponding upper and lower quartiles. The local noon and local night are also indicated with open and solid circles near the abscissa, respectively.

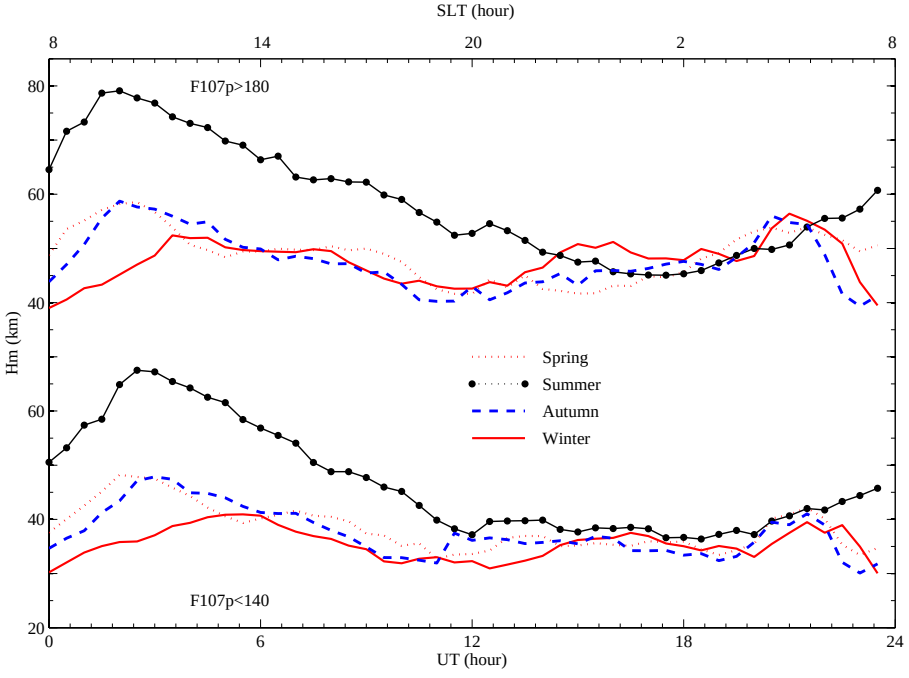

Fig. 4. Diurnal variations of Hm for seasons under high (F107p>180) and moderate-to-low (F107p<140) solar activity levels. Here the solar proxy is F107p = (F107+F107A)/2, where F107A is the 81-day running mean of daily F107 index.

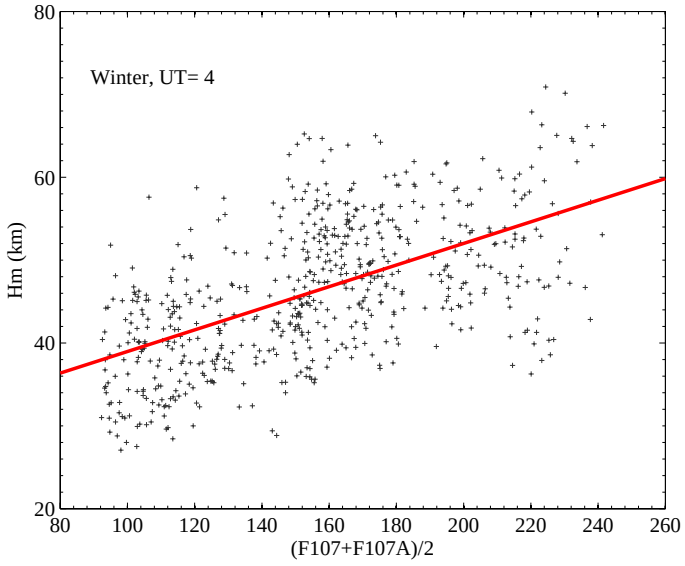

Fig. 5. Scatterplot of the scale height Hm versus the solar activity index F107p at 04:00 UT in winter. The solid line shows the trend of the linear regression.

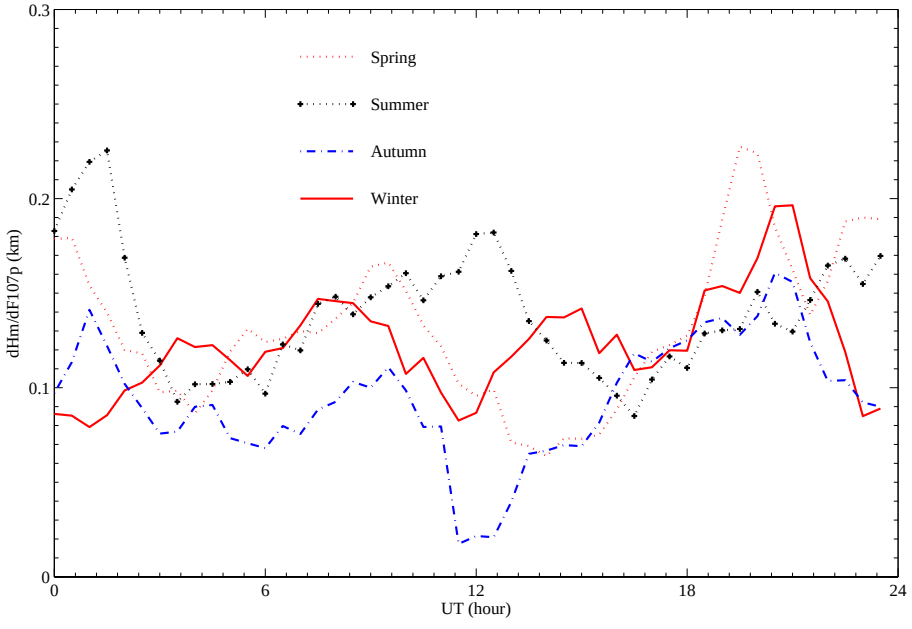

Fig. 6. Diurnal variations of the rate of Hm increase with F107p in four seasons. Here the solar proxy is F107p = (F107+F107A)/2, where F107A is the 81-day running mean of the daily F107 index.

notable diurnal variation with a maximum around 10:00 LT and a minimum around midnight. Both under high and moderate-to-low solar activity, Hm is at its minimum during nighttime. The winter peak of Hm shifts to local midday under high solar activity and even later under moderate-to-low solar activity. The diurnal variation of seasonal median Hm is not so appreciable in other seasons as that in summer. An evident feature found in Figs. 3 and 4 is that the mean daytime values of Hm are highest in summer and lowest in winter, while insignificant seasonal differences are seen in the nighttime Hm. During the daytime, the observed Hm values in summer are about 20 km larger than those in other seasons.

According to Huang and Reinisch (2001), there is a good correlation between Hm and the slab thickness of the ionosphere, which is defined by the ratio of ionospheric total

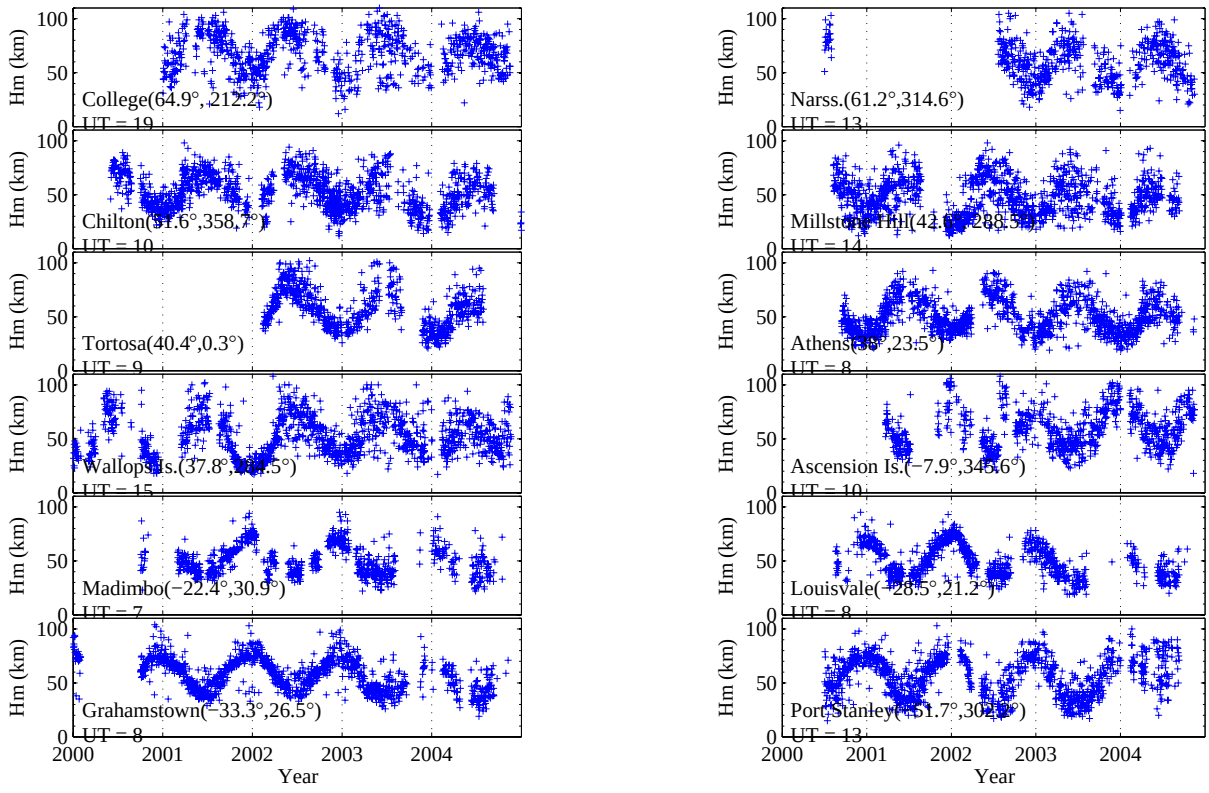

Fig. 7. Time sequences of values of scale height (Hm) at *hm*F2 over 12 stations at specified day times during 2000–2004. The names and their locations of the stations are labeled.

electron content to the peak density. The seasonal feature of Wuhan Hm is also similar to the general trend for the slab thickness to decrease from summer to equinox to winter as reported by Goodwin et al. (1995), Jayachandran et al. (2004) and Wu et al. (1998).

It is evident that the solar activity level should have an influence on Hm. Figure 5 gives a scatterplot of Wuhan Hm versus F107p at 04:00 UT in winter. Although the data set has not covered a full solar cycle, the solar activity index F107 during the observations extends from the minimum of 80 to the maximum of 285.5 (on 28 September 2001), with a mean value of 157. In order to study the solar activity variations of Hm, we investigate the relationship between Hm and F107p at each specified time for the four seasons. It dindicates that the overall trend of the Hm change is a linear increase with respect to F107p, namely the values of Hm tend to be higher for higher solar activities. Thus, the solar dependence of Hm may be represented with the rate of increase with solar flux, dHm/dF107p. Figure 6 demonstrates dHm/dF107p against universal time for the four seasons. The value of dHm/dF107p averages at 0.13 km per solar flux unit by day and night.

If the scale height in an α-Chapman function represents the scale height of the neutral atmosphere, the plasma scale height should be roughly twice as large as the Reinisch and Huang (2004) method. The neutral temperature Tn at Wuhan, provided by the MSIS model (Picone et al., 2002), is shown in the fifth panel of Fig. 8. It is obvious that Hm is not strongly connected with Tn. It is also true for electron or ion temperatures, because there is a significant morning rise in electron and ion temperatures in the F-layer (Oyama et al., 1996; Sharma et al., 2005), while it does not occur in Hm.

It should be mentioned that the classical scale height is defined as kT/mg (here k is the Boltzmann constant, T is the temperature, m is the mass and g the gravitation acceleration), while the scale height Hm, derived from ionograms, is actually a measure of the slope of the topside electron number density profile with a Chapman function, thus it does have not the classical physical meanings. This point has been made by Huang and Reinisch (2001). But Hm derived from the ionograms has some physical meanings. First, the ionogram derived Hm is a measure of the $N_e(h)$ profile, thus it may be thought of as an index for the slope of the topside ionosphere. It has values in topside $N_e(h)$ modeling applications. Second, this Hm is also a measure of slab thickness, although their values may be different from each other, according to the statistical study of Huang and Reinisch (2001) on *Nm*F2, TEC and Hm. In addition, although the Chapman theory can only be applied in the E- and F1-layer, the distribution of the electron density of the topside ionosphere

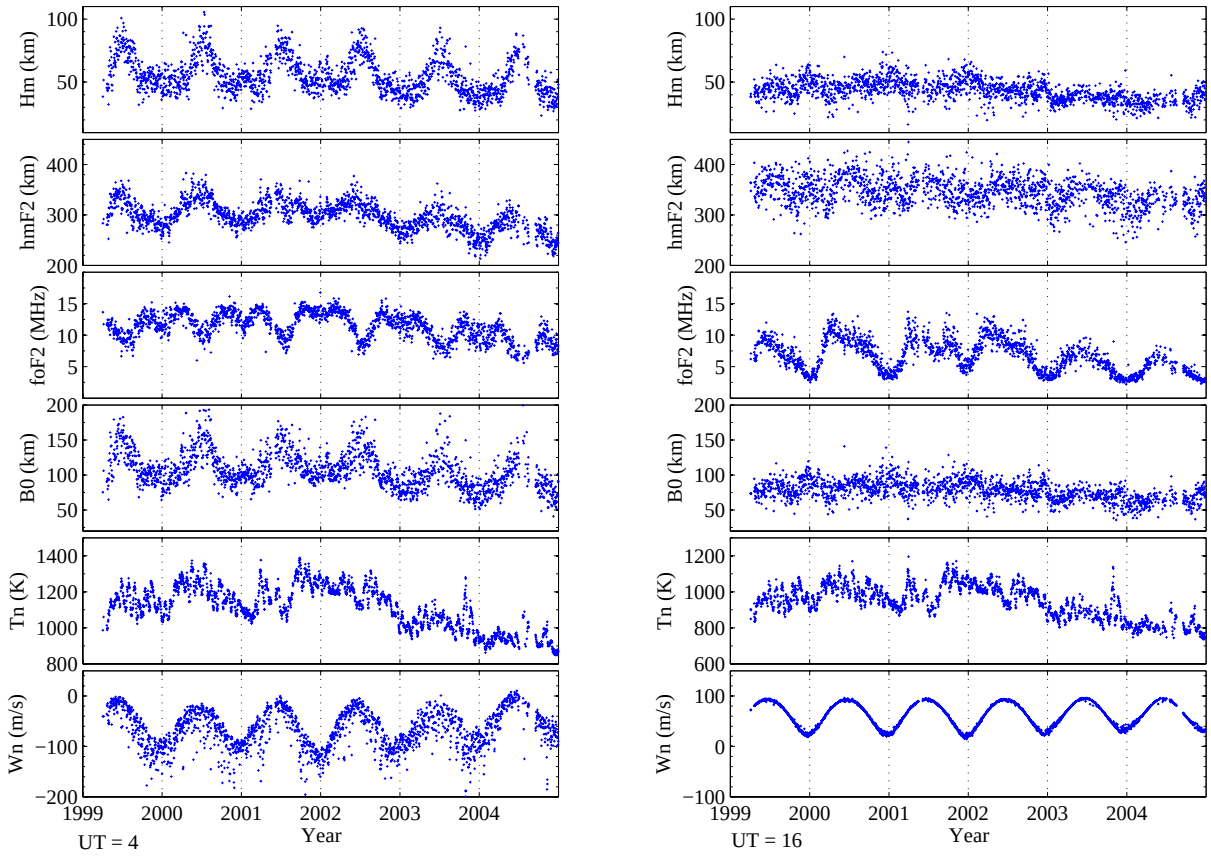

Fig. 8. Time sequences of values of scale height Hm, *fo*F2, *hm*F2, B0, thermospheric temperature Tn (at the height of *hm*F2 from MSIS model), and southward neutral wind Wn (at the height of *hm*F2 from HWM model) over Wuhan at 04:00 UT (left) and 16:00 UT(right) during 1999–2004.

not far away from the F-layer peak can be well described by the Chapman function. Thus, the ionogram derived Hm should contain information on the ionospheric chemical and dynamic processes. This point deserves further investigation.

3.3 Annual variation of Hm at 13 stations

The Earth's ionosphere is known to undergo a yearly variation (e.g. Kawamura et al., 2002; Yu et al., 2004). It is well known that in some parts of the world the predominant variation of *fo*F2 is semiannual, but elsewhere it is significantly annual, usually with a winter maximum (e.g. Torr and Torr, 1973; Yu et al., 2004). To investigate the yearly variation of Hm, besides Wuhan, data at College, Narssarssuaq, Chilton, Millstone Hill, Tortosa, Athens, Wallops Is., Ascension Is., Madimbo, Louisvale, Grahamstown and Port Stanley were also collected. Hm data at these 12 ionosonde stations can be available on the SPIDR web. The latitude of these stations varies from 64.9° N to 51.7° S.

An interesting feature of daytime Hm, which occurs at all latitudes, is its significant annual variation with a summer maximum. Figure 7 shows the time sequence of the day-by-day Hm at a specific time during the daytime over these global 12 stations. During the daytime, the annual component is dominant in the yearly variation of Hm.

We choose the Wuhan station as an example to show the yearly variation of Hm and *hm*F2, *fo*F2 and the IRI bottomside profile thickness parameter B0. Figure 8 shows the day-by-day values of these parameters over Wuhan around local noon and midnight, respectively. The yearly variation of Hm at Wuhan also shows the common feature at the other 12 stations. In addition, Hm has a similar phase with that of *hm*F2 and B0 and an opposite one with *fo*F2. At midnight, the yearly variation of *hm*F2 and B0 becomes much weaker and tends to disappear. In contrast, the annual variation of *fo*F2 is predominant with a peak in summer.

Figure 9 illustrates the amplitudes of the annual and semiannual components of Hm, *hm*F2, *fo*F2 and B0 at Wuhan at different times, while Figure 10 represents the annual phase of these parameters at Wuhan. The yearly variation of Wuhan *fo*F2 has notable annual and semiannual components, although its daytime annual phase is in winter, while at night, its annual variation is predominant with a peak in summer. In contrast, the behaviors of Hm, *hm*F2 and B0 are somewhat

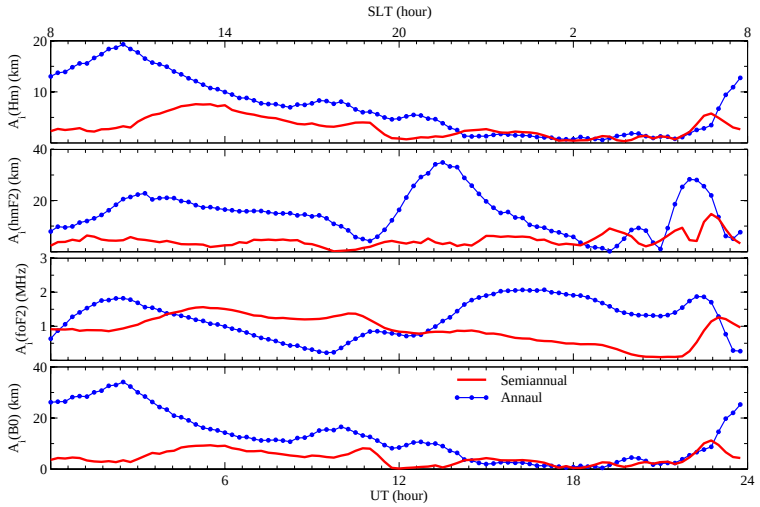

Fig. 9. Amplitudes of annual and semiannual components of Hm, *fo*F2, *hm*F2 and B0 at Wuhan in 2000–2001.

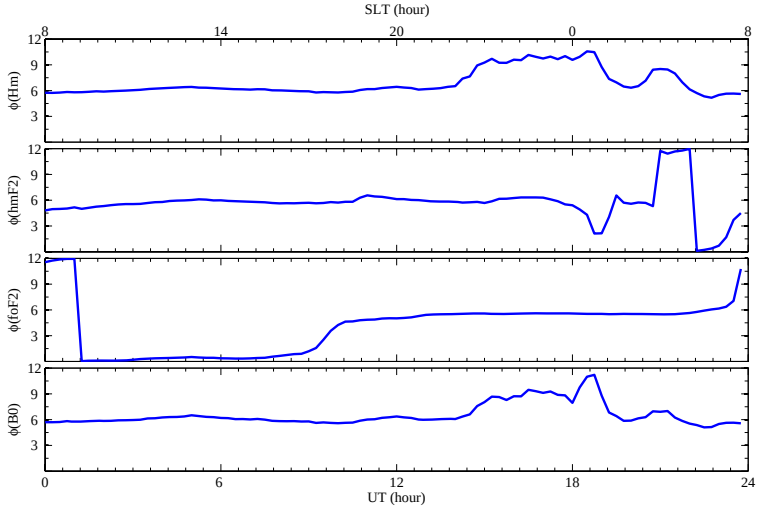

Fig. 10. Phase of the annual component of Hm, *fo*F2, *hm*F2 and B0 at Wuhan in 2000–2001. The phases are in months.

different from that of *fo*F2. Their annual phases are in summer (Fig. 10). As shown in Fig. 9, daytime Hm and *hm*F2 at Wuhan undergo a strong yearly variation with a predominant annual component, while at night the yearly variations become much weaker and tend to disappear. Both the annual and semiannual components of Hm and B0 become insignificant at night.

3.4 The correlation between Hm and *hm*F2, B0

Scatterplots of the scale height Hm versus *hm*F2, *fo*F2 and B0 at Wuhan at local noon (04:00 UT) and midnight (16:00 UT) during 1999–2004 are given in the left and right panels of Fig. 11, respectively. In general, Hm (also B0) shows a moderate positive correlation with *hm*F2 and a very weak negative or poor correlation with *fo*F2.

A striking feature shown in Fig. 11 is the strong correlation between Hm and the IRI bottomside thickness parameter B0 at all local times over Wuhan (with a correlation coefficient as high as 0.92–0.99). Both parameters B0 and Hm are dependent on the shape of the electron density profile in the F region. This dependence justifies the strong correlation between both parameters. Reinisch et al. (2004) discussed the possibility to calculate Hm from the IRI parameters B0, B1 and D1. Their ultimate purpose is searching for an alternate path to an estimate of the topside profile based on the bottomside one. Our result suggests that the strong correlation between Hm and B0 provides a new and convenient way for future modeling of the topside ionospheric shape only from the established B0 parameter set. This point may be helpful for improving the IRI profile prediction in the future.

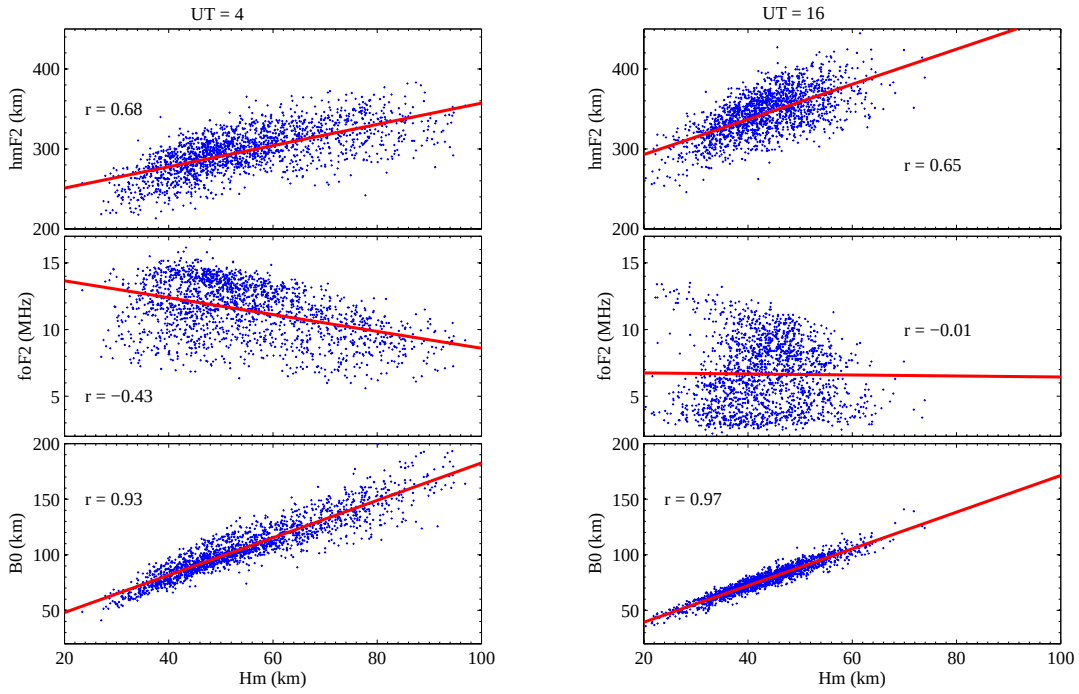

Fig. 11. Scatterplot of the scale height Hm versus *hm*F2, *fo*F2, and IRI thickness parameter B0 at Wuhan around local noon (left, at 04:00 UT) and midnight (right, 16:00 UT) during 1999–2004.

The positive correlation of Hm with *hm*F2 suggests that the physical processes involved in controlling the variation of *hm*F2 may also be responsible for that of Hm. That *hm*F2 greatly depends on the direct effect of horizontal neutral wind is well known from the past and well explained by the theory of the thermospheric winds. Neutral winds and electric fields act to shift the F peak from the balance height to a new level. It is the physical basis of deriving the meridional neutral wind from ionospheric observations (e.g. Rishbeth et al., 1978; Buonsanto et al., 1997; Liu et al., 2003, 2004). The annual variation arises from the summer to winter thermospheric circulation wind. The meridional neutral wind (Wn) for Wuhan around *hm*F2 obtained by the HWM93 model (Hedin et al., 1996) is illustrated in the bottom panel of Fig. 8. As expected, during daytime, the model Wn shows a similar annual pattern as that of *hm*F2 and Hm. It indicates that Wn not only contributes to the ionospheric height but also to the shape of the ionospheric profile. At night, the model Wn still has a significant annual variation, which is far from that of Hm. This point deserves further study, although the current version of the HWM93 model has its limitations.

4 Summary

This paper investigates the diurnal, seasonal, and solar activity variations of the ionogram derived scale height around *hm*F2 observed at Wuhan and the yearly variations of Hm at Wuhan and 12 other stations. The main results are summarized as follows:

(1) It shows that Hm observed at Wuhan has appreciable diurnal and day-to-day variations. Significant disturbances in Hm are presented during geomagnetic active periods. However, the dependence of Hm on magnetic activity is complicated.

(2) The diurnal behaviors of seasonal median Hm under both solar activities are found to be similar. Median values of Hm are highest in summer and lowest in winter during the daytime. At nighttime, Hm exhibits a much weaker seasonal variation. Hm tends to a higher value with increasing solar flux.

(3) A distinct annual variation of Hm is observed at Wuhan and 12 other stations, i.e. Hm has a higher value in summer and a lower value in winter during the daytime. This annual variation becomes much weaker or disappears at the time interval from late night to pre-sunrise.

(4) A strong correlation is found between Hm and the bottomside thickness parameter B0 at all local times. It provides a new and convenient way for modeling the topside ionospheric shape only from the established B0 parameter set. In general, Hm shows a moderate positive correlation with *hm*F2 and negative and little correlation with *fo*F2 depending on the local time.

Acknowledgements. The authors thank two referees for their valuable suggestions for improving the presentation of the paper. The SAO-Explorer software is provided by UMass Lowell Center for Atmospheric Research. The data at global 12 ionosonde stations are downloaded from the Space Physics Interactive Data Resource (SPIDR) web (http://spidr.ngdc.noaa.gov/spidr/). This research was supported by the KIP Pilot Project (kzcx3-sw-144) of Chinese Academy of Sciences and National Natural Science Foundation of China (40574071, 40574072) and National Important Basic Research Project (G2000078407). The author (L. Liu) gratefully acknowledges the support of K. C. Wong Education Foundation, Hong Kong.

Topical Editor M. Pinnock thanks two referees for their help in evaluating this paper.

References

Belehaki, A., Jakowski, N., and Reinisch, B.: Comparison of ionospheric ionization measurements over Athens over Athens using ground ionosonde and GPS derived TEC values, Radio Sci., 38(6), 1105, doi:10.1029/2003RS002868, 2003.

Belehaki, A., Marinov, P., Kutiev, I., Jakowski, N., and Stankov, S.: Comparison of the topside ionosphere scale height determined by topside sounders model and bottomside digisonde profiles, Adv. Space Res., doi:10.1016/j.asr.2005.09.015, in press, 2006.

Bilitza, D.: International reference ionosphere 2000, Radio Sci., 36(2), 261–275, 2001.

Booker, H. G.: Fitting of multi-region ionospheric profiles of electron density by a single analytic function of height, J. Atmos. Terr. Phys., 39, 619–623, 1977.

Buonsanto, M. J., Starks, M. J., Titheridge, J. E., Richards, P. G., and Miller, K. L.: Comparison of techniques for derivation of neutral meridional winds from ionospheric data, J. Geophys. Res., 102, 14 477–14 484, 1997.

Di Giovanni, G. and Radicella, S. M.: An analytical model of the electron density profile in the ionosphere, Adv. Space Res., 10(11), 27–30, 1990.

Goodwin, G. L., Silby, J. H., Lynn, K. J. W., Breed, A. M., and Essex, E. A.: GPS satellite measurements: ionospheric slab thickness and total electron content, J. Atmos. Terr. Phys., 57(14), 1723–1732, 1995.

Hedin, A. E., Fleming, E. L., Manson, A. H., et al.: Empirical wind model for the upper, middle and lower atmosphere, J. Atmos. Terr. Phys., 58(13), 1421–1447, 1996.

Huang, X. and Reinisch, B. W.: Vertical electron profiles from the Digisonde network, Adv. Space Res., 18(6), 121–129, 1996.

Huang X. and Reinisch, B. W.: Vertical electron content from ionograms in real time, Radio Sci., 36(2), 335–342, 2001.

Jayachandran, B., Krishnankutty, T. N., and Gulyaeva, T. L.: Climatology of ionospheric slab thickness, Ann. Geophys., 22, 25–33, 2004.

Kawamura, S., Balan, N., Otsuka, Y., and Fukao, S.: Annual and semiannual variations of the midlatitude ionosphere under low solar activity, J. Geophys. Res., 107(A8), doi:10.1029/2001JA000267, 2002.

Lei, J., Liu, L., Wan, W., and Zhang, S.-R.: Variations of electron density based on long-term incoherent scatter radar and ionosonde measurements over Millstone Hill, Radio Sci., 40, RS2008, doi:10.1029/2004RS003106, 2005.

Liu, L., Luan, X., Wan, W., Ning, B., and Lei, J.: A new approach to the derivation of dynamic information from ionosonde measurements, Ann. Geophys., 21(11), 2185–2191, 2003.

Liu, L., Luan, X., Wan, W., Lei, J., and Ning, B.: Solar activity variations of equivalent winds derived from global ionosonde data, J. Geophys. Res., 109, doi:10.1029/2004JA010574, 2004.

Oyama, K.-I., Watanabe, S., Su, Y., Takahashi, T., and Hiro, K.: Seasonal, local time, and longitudinal variations of electron temperature at the height of ∼600 km in the low latitude region, Adv. Space Res., 18(6), 269–278, 1996.

Picone, J. M., Hedin, A. E., Drob, D. P., and Aikin, A. C.: NRLMSISE-00 empirical model of the atmosphere: Statistical comparisons and scientific issues, J. Geophys. Res., 107(A12), 1468, doi:10.1029/2002JA009430, 2002.

Rawer, K.: Synthesis of ionospheric electron density profiles with Epstein functions, Adv. Space Res., 8(4), 191–198, 1988.

Rawer, K., Bilitza, D., and Gulyaeva, T. L.: New formulas for IRI electron density profile in the topside and middle ionosphere. Adv. Space Res., 5(7), 3–12, 1985.

Reinisch, B. W. and Huang, X.: Automatic calculation of electron density profiles from digital ionograms: 3. Processing of bottomside ionograms, Radio Sci., 18(3), 477–492, 1983.

Reinisch, B. W. and Huang, X.: Deducing topside profiles and total electron content from bottomside ionograms, Adv. Space Res., 27(1), 23–30, 2004.

Reinisch, B. W., Huang, X., Belehaki, A., Shi, J., Zhang, M., and Ilma, R.: Modeling the IRI topside profile using scale height from ground-based ionosonde measurements, Adv. Space Res., 34, 2026–2031, 2004.

Richards, P. G., Fennelly, J. A., and Torr, D. G.: EUVAC: A solar EUV flux model for aeronomic calculations, J. Geophys. Res., 99(A5), 8981–8992, 1994.

Richards, P. G.: Seasonal and solar cycle variations of the ionospheric peak electron density: comparison of measurement and models, J. Geophys. Res., 106(A12), 12 803–12 819, 2001.

Rishbeth, H., Ganguly, S., and Walker, J. C. G.: Field-aligned and field-perpendicular velocities in the ionospheric F2 layer, J. Atmos. Terr. Phys., 40, 767–784, 1978.

Sharma, D. K., Rai, J., Israil, M., and Subrahmanyam, P.: Diurnal, seasonal and longitudinal variations of ionospheric temperatures of the topside F region over the Indian region during solar minimum (1995–1996), J. Atmos. Solar-Terr. Phys., 67, 269–274, 2005.

Stankov, S. M., Jakowski, N., Heise, S., Muhtarov, P., Kutiev, I., and Warnant, R.: A new method for reconstruction of the vertical electron density distribution in the upper ionosphere and plasmasphere, J. Geophys. Res., 108(A5), 1164, doi:10.1029/2002JA009570, 2003.

Torr, M. R. and Torr, D. G.: The seasonal behaviour of the F2-layer of the ionosphere, J. Atmos. Terr. Phys., 35, 2237–2251, 1973.

Wu, J., Long, Q., and Quan, K.: A statistical study and modling of the ionospheric TEC and the slab thickness with observations at Xinxiang, China, Chinese J. Radio Sci., 13(3), 291–296, 1998.

Yu, T., Wan, W., Liu, L., and Zhao, B.: Global scale annual and semi-annual variations of daytime NmF2 in the high solar activity years, J. Atmos. Solar-Terr. Phys., 66, 1691–1701, 2004.